Modelling muscle motor conformations using low-angle X-ray diffraction

J.M. Squire, H.A. AL-Khayat, J.J. Harford, L. Hudson, T. Irving, C. Knupp and M.K. Reedy

Abstract: New results on myosin head organization using analysis of low-angle X-ray diffraction patterns from relaxed insect flight muscle (IFM) from a giant waterbug, building on previous studies of myosin filaments in bony fish skeletal muscle (BFM), show that the information content of such low-angle diffraction patterns is very high despite the 'crystallographically low' resolution limit (65 Å) of the spacings of the Bragg diffraction peaks being used. This high information content and high structural sensitivity arises because: (i) the atomic structures of the domains of the myosin head are known from protein crystallography; and (ii) myosin head action appears to consist mainly of pivoting between domains which themselves stay rather constant in structure; thus (iii) the intensity distribution among diffraction peaks in even the low resolution diffraction pattern is highly determined by the high-resolution distribution of atomically modelled domain mass. A single model was selected among 5000+ computer-generated variations as giving the best fit for the 65 reflections recorded within the selected resolution limit of 65 Å. Clear evidence for a change in shape of the insect flight muscle myosin motor between the resting (probably like the pre-powerstroke) state and the rigor state (considered to mimic the end-of-powerstroke conformation) has been obtained. This illustrates the power of the low-angle X-ray diffraction method. The implications of these new results about myosin motor action during muscle contraction are discussed.

1 Introduction

1.1 Questions being asked

The myosin heads in muscle (Myosin II) are the classic actin-binding motors that were first studied several decades ago [1]. Although it is now known that there are 20 different classes of the myosin superfamily in cells, together with a host of related proteins (e.g. kinesin, dynein, ncd) which interact with microtubules rather than with actin, the behaviour of Class II myosin in muscle remains a major and wonderfully accessible topic for study; myosin II behaviour continues to illuminate the actions of many of these other motors. Nowadays excellent methods are available with which to study the behaviour of single molecules so that in principle any motor molecule can be studied in this way. However, these techniques can only provide a certain kind of information. In particular they do not provide structural information about how the motors change shape during the force-producing process. Microtubule-associated motors can be studied successfully by electron microscopy and image processing combined with results on molecular shape from protein crystallography [2, 3]. However, electron microscopy by its very nature is not a dynamic technique; it can only record snapshots of either equilibrium molecular states or transient states trapped by freeze-fixation. If one poses the question: 'How can I follow structural changes in motor molecules in real time and with high spatial sensitivity?' one of the few available techniques is, in fact, time-resolved low-angle X-ray diffraction and this can only be done on a bulk material like muscle [4, 5], where it gives more global but less site-specific data than spin-label or fluoresence probes [6, 7]. Here we discuss the application of this X-ray technique to the superbly lattice-ordered myosin II motors in insect flight muscle and bony fish muscle, we show results using this technique that are crystallographically rigorous and consistent with structural results from other techniques, and we discuss their implications in terms of the contractile cycle of the myosin II motor on actin.

1.2 Essential features of the myosin II cycle on actin

The muscle acto-myosin ATPase scheme, originally devised by Lymn and Taylor [8], based on the structural ideas of Huxley [1] and others [9, 10]

$$\mathbf{A} + \mathbf{M}.\mathbf{ADP}.\mathbf{Pi} \leftrightarrow \mathbf{AM}.\mathbf{ADP}.\mathbf{Pi} \leftrightarrow \mathbf{AM}.\mathbf{ADP} \leftrightarrow \mathbf{AM} \leftrightarrow \mathbf{A} + \mathbf{M}.\mathbf{ATP} \leftrightarrow \mathbf{A} + \mathbf{M}.\mathbf{ADP}.\mathbf{Pi}$$

(A = actin, M = myosin) currently envisages the energy-releasing steps of early phosphate (Pi) and later ADP release as being coordinated with a forceful one or two-step tilt of the elongated myosin heads while attached to actin, thus causing the actin and myosin filaments to slide past each other.

Myosin II molecules (Fig. 1*a*) consist of a long rod-shaped tail (a two-chain α-helical coiled-coil) on one end of which the chains diverge to form the two comma-shaped myosin head motors. The so-called myosin heavy chain forms the rod and the bulk of each head. The heads also

IEE Proceedings online no. 20031094

doi:10.1049/ip-nbt:20031094

Paper first received 24th April 2003 and in revised form 6th October 2003

J.M. Squire, H.A. AL-Khayat, J.J. Harford, L. Hudson and C. Knupp are with the Biological Structure & Function Section, Biomedical Sciences Division, Faculty of Medicine, Imperial College London, Exhibition Road, London SW7 2AZ, UK

T. Irving is with the BioCAT, Dept. Biological, Chemical and Physical Sciences, Illinois Institute of Technology, Chicago IL 60616, USA

M.K. Reedy is with the Dept of Cell Biology, Duke University, Durham NC 27710, USA

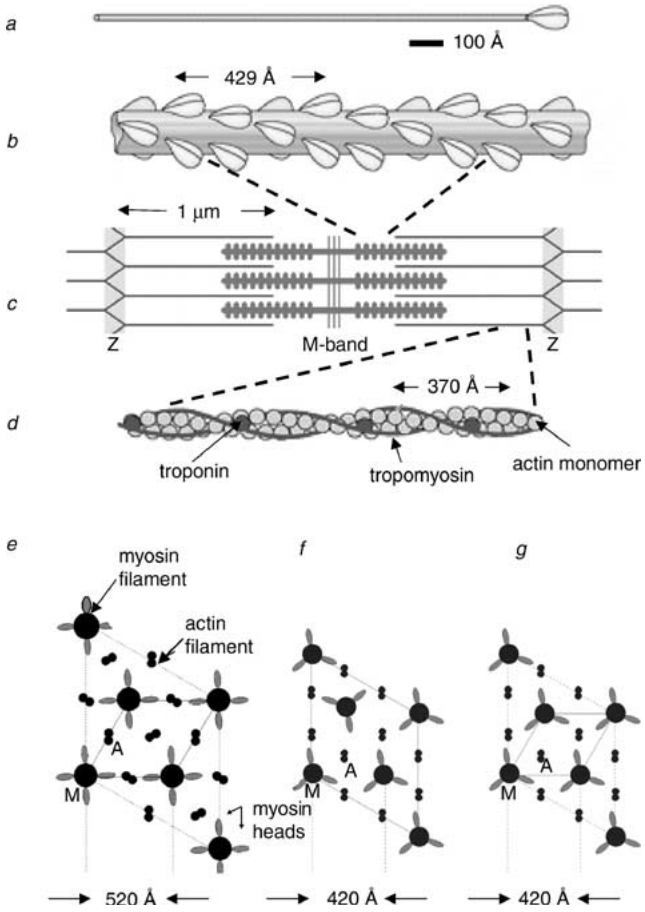

Fig. 1 *Components of striated muscle and their arrangements in the sarcomeres of different striated muscle types*

a Myosin II molecule (muscle form of myosin), consisting of long α-helical coiled-coil rod on the end of which are two globular myosin heads. The structure of the heads is shown in Fig. 2*a*

b Part of a vertebrate muscle myosin filament such as found in BFM, showing how multiple myosin rods are packed into the filament backbone allowing myosin head pairs to emerge on the filament surface in a roughly helical array

c Arrangement of myosin filaments and actin filaments (see (*d*)) to form the muscle repeating unit, the sarcomere. Bipolar myosin filaments are arrayed side-by-side to form the A-band which is crosslinked halfway along at the M-band. The ends of the myosin filaments overlap actin filaments which link to the Z-band (Z-line) and through the Z-band to a similar oppositely directed array of actin filaments in the next sarcomere

d Actin filaments consist of a backbone of actin monomers, each about 50 Å across, arranged on a helix. This appears as two strings of beads slowly twisting around each other. Along each string are arrays of tropomyosin molecules and the troponin complex, which together are involved in the on-off switching by calcium ions (muscle regulation; see [29, 41])

e, *f* and *g* The A-band lattices in cross-sectional view in (e) insect flight muscles (IFM), (f) most vertebrate muscles, including humans, rabbit, rats, mice, chicken, frogs etc and (g) bony fish muscles (BFM). The large circles show the myosin filament backbones and the grey projecting elliptical shapes each represent a pair of myosin heads, four head pairs at each level in IFM (four-fold symmetry (e)) and three head pairs at each level (three-fold symmetry) in vertebrate striated muscles (f, g). See text for further details. (M: myosin, A: actin, Z: Z-band)

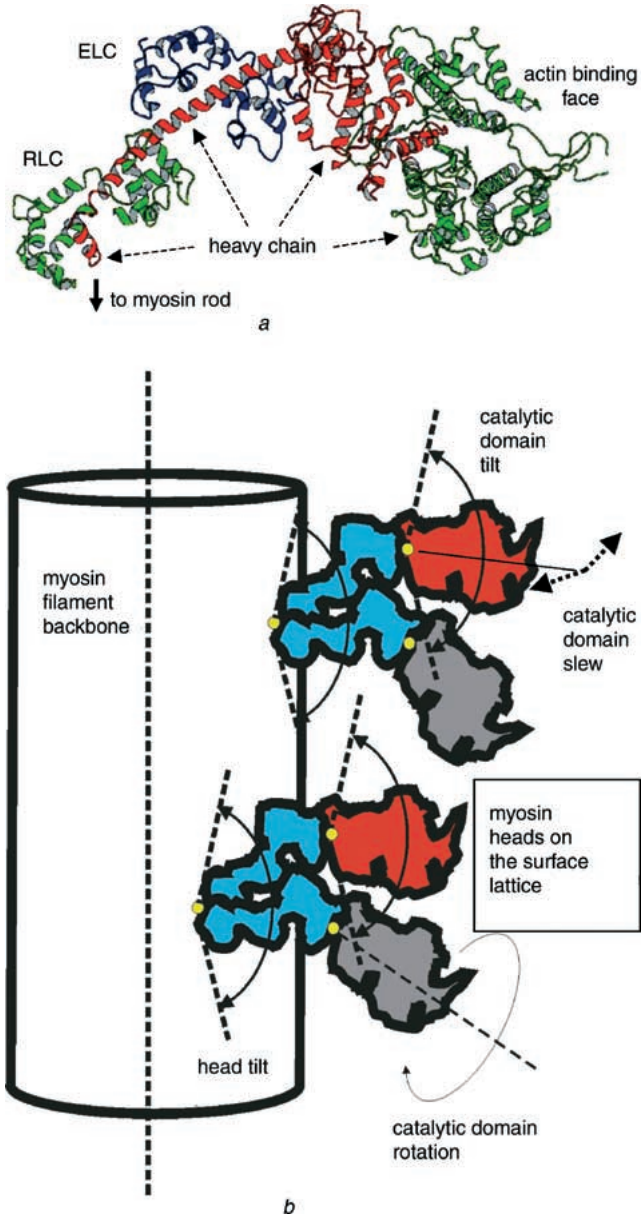

Fig. 2 *Chicken myosin subfragment-1 and myosin heads on a myosin filament*

a Ribbon diagram of the chicken myosin subfragment-1 without nucleotide solved by Rayment *et al.* [17]. The right-hand part (green and some of the red ribbon) is the catalytic (motor) domain which binds ATP and interacts with actin. The heavy chain continues to the left along a rather straight α-helix (red) which bends down at its end where it connects to the myosin rod. Two light chains, the essential light chain (ELC) and the regulatory light chain (RLC), wrap around the long α-helix in the heavy chain. The light chain domain on the left is often termed the neck or the lever arm

b Schematic illustration of the myosin heads on a myosin filament surface showing two pairs of heads and the places in the head where structural changes were modelled. Each head shows an outer motor or catalytic domain (grey or red) and an inner neck region or lever arm (blue). Relative to the origins of the heads on the filament surface, the whole heads could be tilted axially (head tilt) or slewed azimuthally (not illustrated) or rotated around their long axes (not illustrated). In addition, for given positions of the whole head, the catalytic domain could be moved on the end of the lever arm by a further tilt, slew and rotation as illustrated. Systematic searching through these various parameters was carried out by a simulated annealing procedure [30, 31] to give good fits to the observed X-ray diffraction patterns (Fig. 3)

contain two light chains (Fig. 2*a*) that in some muscles regulate on–off switching (muscle regulation) of myosin motor action. The myosin rods pack to form the myosin filament shaft (Fig. 1*b*) with the myosin heads arrayed on the filament surface. In the sarcomere, which is the repeated building block in all striated muscles (Fig. 1*c*) and which, in rest length vertebrate muscles, is about 2.3 μm long

(it is longer in other muscle types), bipolar myosin filaments (i.e. head arrays at opposite ends face in opposite directions) overlap and interdigitate with actin filaments (Fig. 1*d*). Actin filaments are assembled from a helical array of actin monomers along which run polymers of tropomyosin labelled every 390 Å with the calcium-binding protein troponin. The part of the sarcomere containing myosin filaments is known as the A-band. It is bisected by the M-band at which adjacent myosin filaments are crosslinked. Arrays of actin filaments at the sarcomere ends are connected to similar arrays of opposite polarity in the next sarcomeres by crosslinking structures known as Z-bands. The sarcomere runs from one Z-band to the next. Although individual peptide chains in each of these myofibrillar proteins are covalently linked within each molecule, only much weaker protein–protein interactions (e.g. van der Waals, electrostatic and hydrophobic forces) come into play for filament self-assembly, muscle regulation and the force-generating myosin–actin interaction.

In a cross-section through the overlap region of the sarcomere, the myosin and actin filaments have different arrangements depending on the muscle type. Some vertebrate striated muscles, such as our own and those of other higher vertebrates, have the lattice arrangement as in Fig. 1*f*. The myosin filaments have the heads of three myosin molecules around the filament backbone at any one level (Fig. 1*b*), thus giving the vertebrate muscle myosin filament three-fold rotational symmetry, and these filaments are arranged on a hexagonal lattice. Actin filaments, shown as double filled circles, are at the points (so-called trigonal points) at the centre of the triangles formed by three adjacent myosin filaments. By contrast, the A-band lattices in asynchronous (the most prevalent type of) insect flight muscles, shown in Fig. 1*e*, contain myosin filaments which have four-fold rotational symmetry (i.e. heads of four myosin molecules at each axial position) and the actin filaments are located mid-way between two adjacent myosin filaments. The present study focuses on such insect flight muscles and also on the muscles from bony fish. It can be seen in Fig. 1*e* that the four-fold symmetric myosin filaments all have identical rotational orientations around their long axes [11, 12]. In other words insect flight muscle has a very highly ordered arrangement of filaments in three dimensions. However, looking at Fig. 1*f*, for higher vertebrate muscles, it can be seen that the three-fold symmetric myosin filaments can have different rotations (orientations) around their long axes. In fact there are two different orientations, 60° apart, and these orientations are not mixed or alternated in any regular pattern. It turns out that disorder of this type prevails across the muscle A-band lattices of most vertebrate muscles [13, 14], including human muscles and also the frog and rabbit skeletal muscles most widely used in studies of muscle contraction, and this disorder is very unhappy news because of the difficulties and limits it imposes on structural studies. However, there is one exception. This is shown in Fig. 1*g* and refers to the A-band lattices in the muscles of bony fish. These are very much like the A-bands from other vertebrates except that the three-fold symmetric myosin filaments here all have identical rotational orientation. Just as for the insect flight muscles, the myosin filaments in bony fish muscles are also highly ordered in three dimensions; a great advantage in structural studies. It is because of this beautiful lattice order that our studies have concentrated on X-ray diffraction analysis of insect flight muscle and bony fish muscle, which will be referred to from this point on as IFM and BFM, respectively.

As far as the myosin heads are concerned, the M.ADP.Pi state is probably the most populated state in resting muscle [15, 16] and, as discussed below, the heads in this state in IFM and BFM are well ordered in helical or quasi-helical arrays on the myosin filament surface. Myosin heads that are attached to actin with no ATP present (e.g. the AM state) or with only ADP present (the AM.ADP state) form a strong and long-lived interaction which is only broken when ATP rebinds to the heads. Loss of ATP resynthesis from ADP and Pi after death causes an accumulation of long-lived AM and AM.ADP attachments, crosslinking the A-band and making the muscle stiff, to give rise to 'rigor mortis'; the AM state is often referred to as 'rigor'.

1.3 Previous results from protein crystallography and their implications

After postulation of the mechanical crossbridge cycle on actin by Huxley [1] and the biochemical cycle by Lymn and Taylor [8], great efforts were made to purify and crystallise myosin heads so that their structure could be determined by protein crystallography. However, it was not until the work of Rayment *et al.* in 1993 that this was achieved. Their classic paper [17] showed the structure of myosin heads in the absence of nucleotides. This shape could be fitted closely into the myosin density of 3D electron microscopic reconstructions of actin filaments decorated with isolated rigor-state myosin heads [18, 19], but required some bending and twisting to fit into muscle (rigor-state IFM), because lattice-tethered myosin crossbridges capture a variety of strained shapes when attaching to actin [20].

What the Rayment *et al.* structure showed (Fig. 2*a*, [17]) was that the globular part of the comma-shaped myosin head consisted entirely of part of the myosin heavy chain, with its actin-binding face roughly opposite to the ATP-binding site. The heavy chain then continued as an 85 Å long straight α-helical extension, embraced by two light chains in tandem, before converging Y-like towards the same region of its partner head to form the coiled-coil of the myosin rod. Since then a number of other myosin head crystal structures have been published [e.g. 21–24]. The globular domain of the head has been variously known as the 'motor domain' or the 'catalytic domain' and the long α-helix with light chains bound to it has been referred to as the 'neck region', the 'light-chain binding region' or the 'lever arm'. The latter name was introduced to indicate how the new atomic model had modified the original 1969 Huxley proposal for myosin-actin motor action [1] in which the whole head swings on actin; now the movement associated with Pi and ADP release from myosin became envisaged as a change in tilt of the neck part of the head relative to a catalytic domain firmly (stereospecifically) docked on actin [19, 25]. The initially attached state AM.ADP.Pi was often referred to as the weak-binding state since in solution this is a rapidly reversible step, whereas the force-generating AM.ADP state and rigor-like AM state were referred to as strong-binding. An implication of the term strong-binding is that the myosin catalytic domain interaction with actin is stereo-specific (i.e. has a fixed geometry), whereas the initial weak-binding state shows much less stereo-specificity.

After Rayment *et al.* [19] had originally suggested this 'swinging neck' or 'swinging lever arm' scheme for the action of the myosin II motor, several efforts were made to try to crystallise myosin heads in nucleotide-bound states resembling the initial weak-binding or pre-power stroke

state before Pi release. This was eventually achieved using ATP analogues such as ADP.AlF_4 and ADP.VO_4. These new crystal structures showed that the myosin neck or lever arm really can exist in different conformations on the catalytic domain. More crucially, the changes appeared to be relatively simple swings of an unchanging lever arm structure around a fulcrum opposite the actin-binding face of the catalytic domain. The fact that the myosin head behaves roughly as two relatively rigid domains, changing their relative alignment but not their intrinsic shape, means that myosin head conformation in muscle is amenable to modelling from low-angle X-ray diffraction data. If the two domains of the myosin head were to change significantly in shape and not just alignment between the crystal structures of the two states, there would be no manageable limit on the parameters needed to compute derived and related head structures that might be tested for a better fit to the low-angle X-ray diffraction data from muscle.

2 Application of low-angle X-ray diffraction

2.1 Comparison of low-angle X-ray diffraction patterns from relaxed BFM and IFM

Figure 3 compares the low-angle resting state X-ray diffraction patterns from living BFM ([26]: whole muscle, Fig. 3*a*) and IFM ([27]: fibre bundle, Fig. 3*b*). Both patterns show not only very clear sets of horizontal lines of intensity (layer lines), indicating regular arrays of structure along myosin and actin filaments, but also very clear sampling of these layer lines along vertical lines (row lines), indicating that adjacent filaments are themselves organised in a regular 3D fashion over quite large distances. As discussed above, of the muscles known from all studied groups of invertebrate animals, IFM of the asynchronous type

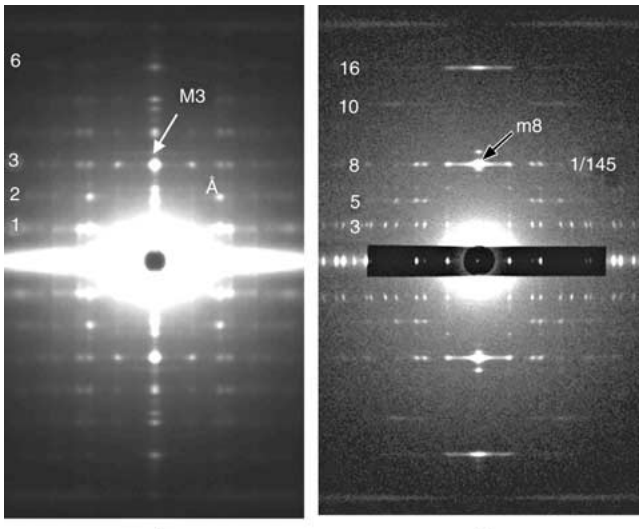

Fig. 3 *X-ray diffraction patterns from BFM (a) and IFM (b) showing the horizontal layer lines and vertical row lines which indicate the presence of good three-dimensional order in both muscles*
The layer line indexing on the left of (*a*) is based on a 429 Å axial repeat. M3 is the meridional reflection on the 3rd layer line of this repeat at 143 Å. The layer line indexing in (*b*) is based on the long repeat of 1160 Å, which is eight times the strong meridional spacing at 145 Å. See [30] and [31] for further details of the X-ray diffraction analysis. Note that the horizontal darker patch halfway up in (*b*) is where a metal absorbing strip (attenuator) was placed along the equator of the diffraction pattern so that the whole pattern recorded on the detector was not swamped by the very strong equatorial reflections

discussed here is the most highly ordered of all (see also [29]; Chapter 8). In this muscle type, oscillatory stretch activation rather than neural input rhythm drives the wing-beat rhythm in flight (see [28]). Likewise, in all the vertebrate species so far studied, BFM is the most highly ordered vertebrate muscle [14]. It is because of the beautiful order in these two chosen muscle types that the probing of muscle action through the low-angle X-ray diffraction method is so potent.

2.2 Proper extraction of muscle diffraction data

In the analysis of the X-ray diffraction patterns in Fig. 3, the first task is to strip from the two-dimensional images of diffracted intensity those parts of the images that actually come from the structures in the muscle that need to be determined (myosin filaments only at this stage). Inevitably there is background scatter from soluble proteins and non-ordered structures in the muscles as well as from the bathing medium and the X-ray cameras themselves (although present-day electronic imaging detectors (CCDs, etc.) can subtract background and otherwise bypass much of the noise and variation inherent in former film-based X-ray recording methods). Not only does this background need to be estimated and removed, but most muscles have some disorientation of their fibres, giving rise to arcing of the observed reflections, the X-ray beam itself has finite size, and the size of the coherent scattering units in the muscle can vary. The task is to estimate accurately the integrated intensity above background within each of the spots (Bragg peaks) in the diffraction patterns. This can be done, for example, by applying image processing software such as that developed specifically to analyse diffraction from non-crystalline and paracrystalline objects by CCP13 (www.ccp13.org). This can estimate and remove the background and then model the peak shapes and fibre disorientation to give a set of reliable intensity values with estimated uncertainties for each peak. For details of these procedures see [30–33]. Once this has been done, the next task is to produce a structural model that can explain these observed intensities.

2.3 Rigorous and objective modelling of observed diffraction data

Diffraction patterns of the kind in Fig. 3 can only be modelled if there is some prior knowledge about the structures involved. Previous painstaking work on relaxed state myosin filaments both from vertebrate muscles, including BFM, and from IFM has shown that they are different even though they have some common features [11, 12, 34–42]. All myosin filaments that have been studied so far appear to show an axial periodicity of around 143 to 145 Å ([29], Chapter 9). The myosin heads occur in rings (so-called crowns) around the roughly cylindrical myosin filament backbones. It is these crowns that are axially separated by 143 to 145 Å. Vertebrate muscle myosin filaments (Fig. 1*b*, *f*, *g*) have the heads of three myosin molecules in each crown and successive 143 Å spaced crowns are rotated around the filament axis by 40° giving an axial repeat after three crowns of 429 Å ($=3\times143$ Å; Fig. 1*b*). In IFM (giant waterbug) each crown contains four pairs of heads (Fig. 1*e*) and successive 145 Å spaced crowns are rotated by 33.75° around the filament axis to give an axial repeat after eight crowns of 1160 Å ($=8\times145$ Å). Fig. 3 shows the observed layer lines in X-ray patterns from the two muscle types indexed as orders of these two repeats.

The presumption in our modelling (Fig. 2*b*) is that, in each myosin head pair, the relaxed myosin heads can move around in three dimensions on their myosin rod tether at the filament surface, unaffected by any interaction with actin. The modelled heads can also change their shape by changing the relative positions of the catalytic domain and the lever arm. If we allow the heads to do this and then compute the diffraction patterns from each head conformation we can compare the observed and calculated intensities and gradually search for the head arrangement which gives the best fit to the observations. This requires considerable computing time, but can be speeded up using an algorithm known as simulated annealing [30]. In this process the myosin head positions are defined in terms of a number of parameters (e.g. tilt, slew, rotation) and the simulated annealing program repeatedly and randomly selects in-range values for these parameters following an 'annealing' schedule, calculating the myosin filament part of a fibre diffraction pattern for each arrangement. It compares the observed and calculated intensities for all the diffraction spots of interest by means of a crystallographic 'goodness-of-fit factor' (R-factor) and then uses the annealing schedule to find the parameter values that give the best myosin head position and shape (lowest R-factor). To check the validity of the result it is normal practice to do the search several times with quite different starting values for the various head parameters. In principle, these searches should then all home in on the same best structure. In practice, this approach can use any starting head shape including any one of the different shapes observed by X-ray crystallography [17, 21–24]. However, using any one of these crystallographically determined head shapes as the starting structure leads to the same best-fit final structures described here because every computational search explores a full range of randomly generated (annealed) internal head shapes (passing through any of the other observed crystallographically determined head shapes) as well as the full range of head positions in space. In both studies [30, 31] all the heads in a given filament were assumed to have the same shape in any one of the many thousands of models generated in each search, differing between all models that tested a given head position, but identical for all position trials of a given head shape. With further development of the program, the two heads of each myosin molecule will be allowed to adopt different shapes within a single test model.

3 Results and discussion

3.1 Myosin head configurations in relaxed insect and fish striated muscles

Figure 4 shows reconstructions of the best relaxed myosin head array models for (a) BFM; plaice fin muscle [30, 43] and (b) IFM; giant waterbug (*Lethocerus*) flight muscle [31]. Details of these analyses are given in the cited references. The general rotational and helical symmetry of each best-fit model remains as originally specified and summarised under 'Rigorous and objective modelling …' (section 2.3). However, note that in BFM myosin filaments (Fig. 4*a*) the head arrangement is not perfectly helical; each crown level within the 429 Å repeat is different. This is a well-known head perturbation in resting vertebrate striated muscle [1, 26]. The IFM myosin filaments (Fig. 4*b*), in contrast, appear to be perfectly helical.

Scrutiny of the head arrangements in Fig. 4 shows that the two heads in one myosin molecule in vertebrate (BFM) myosin filaments are close to each other and in two of the three crowns appear to nest together with the catalytic

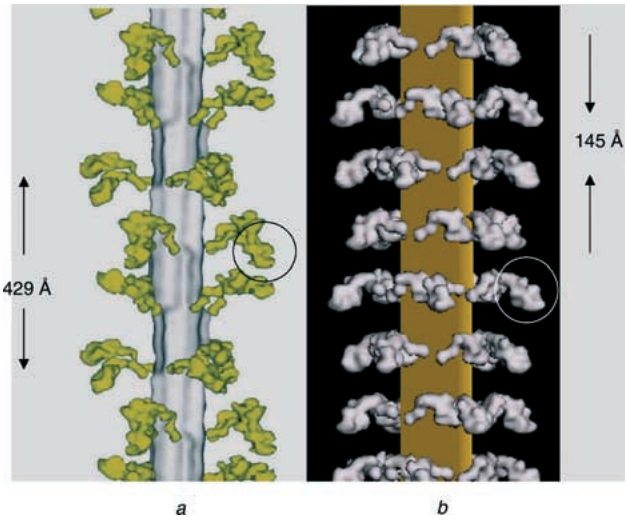

Fig. 4 *The best structures for the myosin head arrangements in relaxed BFM (plaice fin muscle) (a) and in relaxed IFM (Lethocerus) (b) are shown as density reconstructions based on models arrived at by simulated annealing searches as described in Fig. 2*

In both cases the M-band direction is at the bottom. The circled myosin heads show similar spatial positions for the catalytic domains even though the head shapes and arrangements in (*a*) and (*b*) are quite different. (Figure based on data from [30, 31]; In the case of BFM the searches involved optimisation of about 22–25 parameters against 56 observed independent intensities, giving an R-factor (goodness of fit factor) of 3.4 % [30]. In the case of IFM the searches involved 13 parameters optimised against 65 independent intensities giving an R-factor of 9.7% [31])

domains one above the other. The best head shape, even allowing the catalytic domain to move relative to the lever arm in the simulated annealing search, is close to the rigor (nucleotide-free) state reported by Rayment *et al.* [17]. In contrast to this, the IFM myosin heads are arranged so that a head from one myosin molecule tucks in behind a projecting head from a neighbouring molecule in the same crown. Once again there is nesting of heads, but this time it is between heads from different molecules. Another striking difference from the BFM structure is that the best model for IFM thick filaments has the head shape very different from the Rayment [17] nucleotide-free conformation. In this case the head shape is much closer to the shapes observed by Dominguez *et al.* [21] and by Houdusse *et al.* [24] for heads carrying ATP analogues that are thought to mimic the pre-powerstroke shape of the head at the start of actin attachment (i.e. to mimic AM.ADP.Pi; smooth muscle myosin [21] had ADP.AlF_4 and scallop muscle myosin [24] had ADP.VO_4). In summary, both the head shapes and the head arrangements are different in the BFM and IFM myosin filaments.

To simplify computation, we initially used a low-resolution model of the myosin head. This comprised 59 spheres (radius 8.61 Å) of uniform and equal density that accurately represented the mass distribution within the domains of the Rayment atomic model. At the resolution being studied this approximate head gave a computed single head diffraction pattern that differed by only 0.5% from the diffraction pattern of the full atomic model. At this voxel resolution of ~17 Å, it appeared likely that the converter domain, a region of the catalytic domain in which the lever arm is 'rooted' and which rotates to drive the lever arm through an active change in its tilt angle, would appear as an undifferentiated ball joint within the catalytic domain whose rotation would not shift any local mass centroid.

However, in particular cases such as the Dominguez *et al.* structure [21] we used the full atomic coordinates to produce a 59 sphere model with a resulting relatively poor R-factor of 17.8%. This compares with R-factors for the Rayment shape of 22.2% and for our own best model (Fig. 4*b*) of 9.7%.

3.2 Conclusions about myosin motor action

Despite the large differences between the IFM and BFM structures there is one feature that stands out. For some of the highest radius heads, circled in Fig. 4, in other words those heads that may be closest to an adjacent actin filament, the motor domains in both filament types are in roughly similar orientations in space; they present roughly the same face to the neighbouring actin filaments, with some variation in rotation about the motor domain axis. Other than this, our resting motor domain presentations (Fig. 5) also emulate reasonably closely the catalytic domain position in rigor heads on actin in 3-D reconstructions (Fig. 5*a* right). Figure 5*b* shows that, in the case of IFM, if a high-radius head on the relaxed myosin filament moves out radially and makes a modest (one-sixth turn) rotation around its origin as a rigid body, it can now present its motor domain to a suitably oriented actin monomer in the same position that the Rayment-model motor domain adopts for rigor attachment. The small rotation brings the motor domain maximally Z-ward, that is, as near to the Z-band (Fig. 1) as it can reach for an actin site without changing its overall pre-powerstroke shape. This leaves the neck angled straight towards the M-band from the motor domain; the lever arm is ideally poised for a purely axial swing of about 100 Å to reach an end-of-powerstroke rigor position. It is almost as if the outer myosin heads in IFM, which is well-known for speed of action in its oscillatory myogenic contractile cycle when driving the insect wingbeat, are precision-poised for rapid actin attachment and rapid head swinging on actin associated with the sequential release of Pi (to initiate force generation) and ADP product release (to clear the fuelling site so it can bind a fresh charge of the energy-rich nucleotide ATP).

It is perhaps a puzzle that the head conformations in resting BFM and IFM, both presumed to be in the M.ADP.Pi states, are actually different. However, it has also been found in different myosin head crystal structures that the same nucleotide or nucleotide analogue can give different structures. This is presumably a reflection of the fact that any re-orientation of the lever arm on the catalytic domain is a redistribution between equilibrium states and that changes in local conditions may shift this equlibrium. Thus species-specific protein–protein interactions between partner heads in muscle, and between purified single heads in the environment of a given crystal unit cell, may contribute decisively and differently, even with the same nucleotide bound, to govern what sectors of the conformational repertoire become accessed and stabilised. There is another point here: the interaction between heads in relaxed IFM thick filaments, where the inner head ATP sites interact with the essential light chains of the outer heads, may possibly be a means of aiding regulation by locking both heads in the off state. The rise in calcium that activates thin filaments sterically, via the troponin–tropomyosin uncovering of myosin-binding sites [29, 41], could help set IFM sarcomeres on the threshold of stretch activation by additional effects on thick filaments, by weakening and poising this interlocking crown structure to enable full and final release of the heads when thick filament backbones are strained by the activating sarcomere stretch of 1–3%. In any case, in both muscle types, having head pairs interacting is clearly a good way of stabilising the outer heads in appropriate orientations for actin binding.

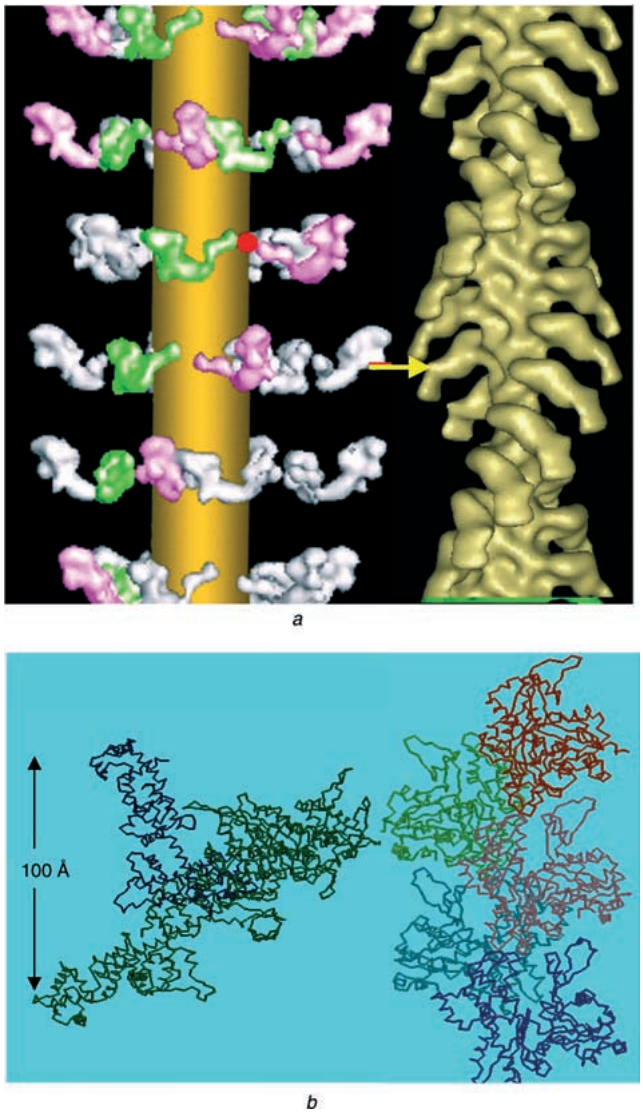

Fig. 5 *Resting motor domain presentations*
The figure to the left of (*a*) is part of the resting IFM myosin filament structure shown in Fig. 4*b*, but it has been turned so that the M-band direction is now upwards, Z-band downwards. Adjacent to it (right) is a 3D reconstruction of an actin filament saturated ('decorated') with myosin heads strongly and stereo-specifically bound in the rigor state. The spatial configurations of the catalytic domain positions of the outermost heads on the relaxed myosin filament and the attached heads in the decorated actin filament are rather similar, but the lever arm positions are clearly very different, and become even more so when the relaxed IFM head rotates around its origin in order to make an exact rigor-like bond with actin This difference is demonstrated in (*b*) where the catalytic domains of the two structures in (*a*) have been superimposed and positioned as if on actin and the lever arm positions are either as in relaxed insect muscle head (upper position (blue); not unlike the structure in Dominguez *et al.* [21]) or as in the Rayment *et al.* [17] rigor shape (lower position, green). The catalytic domain is now oriented as it would be in a decorated actin filament [19] with the actin filament axis vertical (five actin subunits shown on right). The myosin rod end of the lever arm must now move by about 100 Å in a direction parallel to the actin filament axis to reach the rigor-like end-of-powerstroke conformation. (Figure based on data from [31])

3.3 The future – specimen and hardware limitations

The success of our application of low-angle X-ray diffraction to objective modelling of myosin head shape and position in static muscle steady states needs to be followed up with time-resolved X-ray diffraction studies to see the myosin heads in action in active muscle. Comparison and coordination of such detailed myosin head models with direct images of quick-frozen myosin crossbridges in active and other muscle states by tomographic 3D electron microscopy [44] should provide insights that will cross-validate and bootstrap the power of both approaches. Improved X-ray diffraction analysis requires not only the very highest brilliance beamlines at synchrotron X-ray sources, but also the use of very fast readout area detectors such as the RAPID detector at the Daresbury SRS [45]. This detector can be read out in as little as 10 μs; following muscle events on a millisecond or 100 μs timescale can be achieved [4, 46–49 and many others]. Unfortunately, the beam size at the Daresbury SRS is large and the intensity of the X-ray beam is relatively low. The third-generation synchrotron sources such as the ESRF in Grenoble, France, the APS in Chicago, USA and SPring8 in Japan, provide very much more brilliant beamlines (i.e. high intensity in a small beam) but, unfortunately, they do not yet have detectors equivalent to RAPID with which to carry out fast time-resolved experiments. Methods of stripping and modelling the observed X-ray diffraction patterns once they have been recorded are steadily improving especially under the CCP13 project (www.ccp13.org) but new technical developments, especially in the area of fast readout, high spatial resolution area detectors, are needed for the powerful structural technique of time-resolved, low-angle X-ray diffraction to be fully exploited in understanding the action of the molecular motors in muscle and thus producing 'Muscle – the Movie' [50].

4 Acknowledgments

We thank Bruce Baumann for assistance in collecting fibre X-ray diffraction patterns from IFM at the Argonne/ APS/ BioCAT beamline. We acknowledge specific grant support for this work to JMS from the UK BBSRC (28/S10891) and the Wellcome Trust (061729). MKR was supported by NIH AR-14317. CCP13 software was developed as part of UK BBSRC/ EPSRC funded projects (e.g. 28/B10368 and 28/B15281). Use of the Advanced Photon Source was supported by the US Department of Energy, Basic Energy Sciences, Office of Energy Research, under Contract No. W-31-109-ENG-38. BioCAT is a US National Institutes of Health-supported Research Centre RR08630.

5 References

1 Huxley, H.E.: 'The mechanism of muscular contraction', *Science*, 1969, **164**, pp. 1356–1366
2 Hirose, K., Lockhart, A., Cross, R.A., and Amos, L.A.: 'Three-dimensional electron cryo-microscopy of dimeric kinesin and ncd motor domains on microtubules', *Proc. Natl. Acad. Sci. USA*, 1996, **93**, pp. 9539–9544
3 Wendt, T.G., Volkmann, N., Skiniotis, G., Goldie, K.N., Muller, J., Mandelkow, E., and Hoenger, A.: 'Microscopic evidence for a minus-end-directed power stroke in the kinesin motor ncd', *EMBO J.*, 2002, **21**, pp. 5969–5978
4 Harford, J.J., and Squire, J.M.: 'Time-resolved diffraction studies of muscle using synchrotron radiation', *Rep. Prog. Phys.*, 1997, **60**, pp. 1723–1787
5 Squire, J.M.: 'Fibre and muscle diffraction', *in* Fanchon, E., Geissler, E., Hodeau, L.-L., Regnard, J.-R. and Timmins, P. (Eds.) 'Structure and Dynamics of Biomolecules' (Oxford Univ. Press, Oxford, UK, 2000), pp. 272–301
6 Hopkins, S.C., Sabido-David, C., Van Der Heide, U.A., Ferguson, R.E., Brandmeier, B.D., Dale, R.E., Kendrick-Jones, J., Corrie, J.E., Trentham, D.R., Irving, M., and Goldman, Y.E.: 'Orientation changes of the myosin light chain domain during filament sliding in active and rigor muscle', *J. Mol. Biol.*, 2002, **318**, pp. 1275–1291
7 Reedy, M.K., Lucaveche, C., Naber, N., and Cooke, R.: 'Insect crossbridges, relaxed by spin-labelled nucleotide, show well-ordered 90° state by X-ray diffraction and electron microscopy, but spectra of electron paramagnetic resonance probes report disorder', *J. Mol. Biol.*, 1992, **227**, pp. 678–697
8 Lymn, R.W., and Taylor, E.W.: 'Mechanism of adenosine triphosphate hydrolysis by actomyosin', *Biochemistry*, 1971, **10**, pp. 4617–4624
9 Reedy, M.K., Holmes, K.C., and Tregear, R.T.: 'Induced changes in orientation of the crossbridges of glycerinated insect flight muscle', *Nature*, 1965, **207**, pp. 1276–1280
10 Pringle, J.W.S.: 'The contractile mechanism of insect fibrillar muscle', *Prog. Biophys. Mol. Biol.*, 1967, **17**, pp. 1–68
11 Reedy, M.K., Lucaveche, C., Reedy, M.C., and Somasundaram, B.: 'Experiments on crossbridge action and filament sliding in insect flight muscle', *Adv. Exp. Med. Biol.*, 1993, **332**, pp. 33–44
12 Schmitz, H., Lucaveche, C., Reedy, M.K., and Taylor, K.A.: 'Oblique section 3-D reconstruction of relaxed insect flight muscle reveals the cross-bridge lattice in helical registration', *Biophys. J.*, 1994, **67**, pp. 1620–1633
13 Luther, P.K., and Squire, J.M.: 'Three-dimensional structure of the vertebrate muscle A-band. II. The myosin filament superlattice', *J. Mol. Biol.*, 1980, **141**, pp. 409–439
14 Luther, P.K., Squire, J.M., and Forey, P.L.: 'Evolution of myosin filament arrangements in vertebrate skeletal muscle', *J. Morphol.*, 1996, **229**, pp. 325–335
15 Hibberd, M.G., and Trentham, D.R.: 'Relationships between chemical and mechanical events during muscular contraction', *Ann. Rev. Biophys. Biophys. Chem.*, 1986, **15**, pp. 119–161
16 Xu, S., Gu, J., Rhodes, T., Belknap, B., Rosenbaum, G., Offer, G., White, H., and Yu, L. C.: 'The M.ADP.P(i) state is required for helical order in the thick filaments of skeletal muscle', *Biophys. J.*, 1999, **77**, pp. 2665–2676
17 Rayment, I., Rypniewsky, W.R., Schmidt-Bäse, K., Smith, R., Tomchick, D.R., Benning, M.M., Winkelmann, D.A., Wesenberg, G., and Holden, H.M.: 'Three-dimensional structure of myosin subfragment-1: a molecular motor', *Science*, 1993, **261**, pp. 50–58
18 Milligan, R.A., and Flicker, P.F.: 'Structural relationships of actin, myosin, and tropomyosin revealed by cryo-electron microscopy', *J. Cell Biol.*, 1987, **105**, pp. 29–39
19 Rayment, I., Holden, H.M., Whittaker, M., Yohn, C.B., Lorenz, M., Holmes, K.C., and Milligan, R.A.: 'Structure of the actin-myosin complex and its implications for muscle contraction', *Science*, 1993, **261**, pp. 58–65
20 Chen, L.F., Winkler, H., Reedy, M.K., Reedy, M.C., and Taylor, K.A.: 'Molecular modeling of averaged rigor crossbridges from tomograms of insect flight muscle', *J. Struct. Biol.*, 2002, **138**, pp. 92–104
21 Dominguez, R., Freyzon, Y., Trybus, K.M., and Cohen, C.: 'Crystal structure of a vertebrate smooth muscle myosin motor domain and its complex with the essential light chain: visualization of the pre- power stroke state', *Cell*, 1998, **94**, pp. 559–571
22 Houdusse, A., Kalabokis, V.N., Himmel, D., Szent-Gyorgyi, A.G., and Cohen, C.: 'Atomic structure of scallop myosin subfragment S1 complexed with MgADP: A novel conformation of the myosin head', *Cell*, 1999, **97**, pp. 459–470
23 Houdusse, A., and Sweeney, H.L.: 'Myosin motors: missing structures and hidden springs', *Curr. Opin. Struct. Biol.*, 2001, **11**, pp. 182–194
24 Houdusse, A., Szent-Gyorgyi, A.G., and Cohen, C.: 'Three conformational states of scallop myosin S1', *Proc. Natl. Acad. Sci. U S A*, 2000, **97**, pp. 11238–11243
25 Holmes, K.C.: 'Muscle proteins-their actions and interactions', *Curr. Opin. Struct. Biol.*, 1996, **6**, pp. 781–789
26 Harford, J.J., and Squire, J.M.: '"Crystalline" myosin cross-bridge array in relaxed bony fish muscle. Low-angle X-ray diffraction from plaice fin muscle and its interpretation', *Biophys. J.*, 1986, **50**, pp. 145–155
27 Reedy, M.K., Squire, J.M., Baumann, B.A.J., Stewart, A., and Irving, T.C.: 'X-ray fibre diffraction of the indirect flight muscle of Lethocerus indicus', *in* 'Advanced Photon Source User Activity: Report 2000' (Argonne National Laboratory, Argonne, IL, 2000)
28 Josephson, R.K., Malamud, J.G., and Stokes, D.R.: 'Asynchronous muscle: A primer', *J. Exp. Biol.*, 2000, **203**, pp. 2713–2722
29 Squire, J.M.: 'The Structural Basis of Muscular Contraction', (Plenum Press, NY, 1981)
30 Hudson, L., Harford, J.J., Denny, R.C., and Squire, J.M.: 'Myosin head configuration in relaxed fish muscle: resting state myosin heads must swing axially by up to 150 A or turn upside down to reach rigor', *J. Mol. Biol.*, 1997, **273**, pp. 440–455
31 AL-Khayat, H.A., Hudson, L., Reedy, M.K., Irving, T.C., and Squire, J.M.: 'Myosin head configuration in relaxed insect flight muscle: X-ray modelled resting crossbridges in a pre-power-stroke state are poised for actin binding', *Biophys. J.*, 2003, **85**, pp. 1063–1079
32 Squire, J.M., AL-Khayat, H.A., Arnott, A., Crawshaw, J., Denny, R., Diakun, G., Dover, S.D., Forsyth, V.T., He, A., Knupp, C., Mant, G., Rajkumar, G., Rodman, M.J., Shotton, M., and Windle, A.H.:

'New CCP13 software and the strategy behind further developments: Stripping and modelling of fibre diffraction data', *Fibre Diffr. Rev.*, 2003, **11**, pp. 7–19 (see www.ccp3.org)
33 Squire, J.M., Knupp, C., AL-Khayat, H.A., and Harford, J.J.: 'Millisecond time-resolved low-angle X-ray diffraction: a powerful, high-sensitivity technique for modelling real-time movements in biological macromolecular assemblies', *Fibre Diff. Rev.*, 2003, **11**, pp. 28–35 (see www.ccp13.org)
34 Huxley, H.E., and Brown, W.: 'The low-angle X-ray diagram of vertebrate striated muscle and its behaviour during contraction and rigor', *J. Mol. Biol.*, 1967, **30**, pp. 383–434
35 Reedy, M.K.: 'Ultrastructure of insect flight muscle I: screw sense and structural grouping in the rigor crossbridge lattice', *J. Mol. Biol.*, 1968, **31**, pp. 155–176
36 Squire, J.M.: 'General model of myosin filament structure II: myosin filaments and crossbridge interactions in vertebrate striated and insect flight muscles', *J. Mol. Biol.*, 1972, **72**, pp. 125–138
37 Luther, P.K., Munro, P.M.G., and Squire, J.M.: 'Three–dimensional structure of the vertebrate muscle A–band III: M–region structure and myosin filament symmetry', *J. Mol. Biol.*, 1981, **151**, pp. 703–730
38 Squire, J.M.: 'Muscle myosin filaments: Internal structure and crossbridge organisation', *Comments Molec. Cell. Biophys.*, 1986, **3**, pp. 155–177
39 Kensler, R.W., and Stewart, M.: 'An ultrastructural study of the crossbridge arrangement in the fish skeletal muscle thick filament', *J. Cell Sci.*, 1989, **94**, pp. 391–401
40 Morris, E.P., Squire, J.M., and Fuller, G.W.: 'The 4-stranded helical arrangement of myosin heads on insect (*Lethocerus*) flight muscle thick filaments', *J. Struct. Biol.*, 1991, **107**, pp. 237–249
41 Squire, J.M.: 'Architecture and function in the muscle sarcomere', *Curr. Opin. Struct. Biol.*, 1997, **7**, pp. 247–257
42 Eakins, F., AL-Khayat, H.A., Kensler, R.W., Morris, E.P., and Squire, J.M.: '3D structure of fish muscle myosin filaments', *J. Struct. Biol.*, 2002, **137**, pp. 154–163
43 Squire, J.M., Cantino, M., Chew, M., Denny, R., Harford, J.J., Hudson, L., and Luther, P.K.: 'Myosin rod-packing schemes in vertebrate muscle thick filaments', *J. Struct. Biol.*, 1998, **122**, pp. 128–138
44 Taylor, K.A., Schmitz, H., Reedy, M.C., Goldman, Y.E., Franzini-Armstrong, C., Sasaki, H., Tregear, R.T., Poole, K.J.V., Lucaveche, C., Edwards, R.J., Chen, L.F., Winkler, H., and Reedy, M.K.: 'Tomographic 3-D reconstruction of quick frozen, Ca^{2+}-activated contracting insect flight muscle', *Cell*, 1999, **99**, pp. 421–431
45 Lewis, R.A., Hall, C., Parker, B., Jones, A., Helsby, W., Sheldon, J., Clifford, P., Hillen, M., and Fore, N.: 'The "RAPID" high rate area X-ray detector system', *Fibre Diff. Rev.*, 1996, **5**, pp. 30–34 (see www.ccp13.org)
46 Harford, J.J., and Squire, J.M.: 'Evidence for structurally different attached states of myosin cross-bridges on actin during contraction of fish muscle', *Biophys. J.*, 1992, **63**, pp. 387–396
47 Irving, M., Lombardi, V., Piazzesi, G., and Ferenczi, M.A.: 'Myosin head movements are synchronous with the elementary force-generating process in muscle', *Nature*, 1992, **357**, pp. 156–158
48 Martin-Fernandez, M.L., Bordas, J., Diakun, G., Harries, J., Lowy, J., Mant, G.R., Svennson, A., and Townes-Andrews, E.: 'Time-resolved X-ray diffraction studies of myosin head movements in live frog sartorius muscle during isometric and isotonic contractions', *J. Musle Res. Cell Motil.*, 1994, **15**, pp. 319–348
49 Lombardi, V., Piazzesi, G., Ferenczi, M.A., Thirlwell, H., Dobbie, I., and Irving, M.: 'Elastic distortion of myosin heads and repriming of the working stroke in muscle', *Nature*, 1995, **374**, pp. 553–555
50 Squire, J.M., Harford, J.J., and AL-Khayat, H.A.: 'Molecular movements in contracting muscle: towards Muscle – The Movie', *Biophys. Chem.*, 1994, **50**, pp. 87–96